J Therm Anal Calorim (2009) 97:91–98
DOI 10.1007/s10973-009-0080-x

Thermal behaviour of the system $Fe(NO_3)_3 \cdot 9H_2O$–$Bi_5O(OH)_9(NO_3)_4 \cdot 9H_2O$–glycine/urea and of their generated oxides ($BiFeO_3$)

Bogdan Jurca · Carmen Paraschiv · Adelina Ianculescu · Oana Carp

ICTAC 2008 Conference

Abstract Bismuth ferrite ($BiFeO_3$) was obtained by a combustion reaction staring from two precursors systems, namely $Fe(NO_3)_3 \cdot 9H_2O$–$Bi_5O(OH)_9(NO_3)_4 \cdot 9H_2O$–glycine/urea with different metal nitrate/fuel molar ratios. The precursors' thermal behavior is dependent on the fuel nature but practically independent to the fuel content. In glycine containing systems not all Bi_2O_3 is included into mixed oxides during the decomposition. Its presence was identified through the existence of two endothermic phase transitions ($T_{DTA\ max}$ at 745 and 818 °C) assigned to Bi_2O_3 $\alpha \rightarrow \delta$ transition, and its melting. The thermal investigations performed on oxides samples reveal for all oxides, independent on the precursor system, a similar behavior. For all the oxides was identified both the Curie temperature (which decreases with the annealing cycles) and the incongruent melting point (which is with ~10 °C higher for glycine generated oxides comparative with urea ones). The structural analysis shows in the case of the oxides prepared using urea as fuel, a faster evolution toward a single phase composition with the temperature, the formation of the $BiFeO_3$ perovskite phase being completed in the temperature range of 500–550 °C. Only some traces of $Bi_{36}Fe_2O_{57}$ were identified at the detection limit. TEM analysis performed on the $BiFeO_3$ thermally treated at 500 °C for 3 h revealed the presence of small particles with an average size of ~33 nm and polycrystalline agglomerates with an average size of ~100 nm for glycine/urea derived oxides.

Keywords Urea · Glycine · Combustion synthesis · Bismuth iron oxide

B. Jurca
Department of Physical Chemistry, Faculty of Chemistry, University of Bucharest, Bd. Elisabeta no. 12, Bucharest, Roumania

C. Paraschiv
ICPE-CA, Splaiul Unirii no. 313, Bucharest, Roumania

A. Ianculescu (✉)
Department of Oxide Materials Science and Engineering, Faculty of Applied Chemistry and Materials Science, Polytechnic University of Bucharest, Gh. Polizu Street no. 1-7, 011061 Bucharest, Roumania
e-mail: a_ianculescu@yahoo.com

O. Carp
Institute of Physical Chemistry, Splaiul Independentei no. 202, 060021 Bucharest, Roumania

Introduction

Recently, the combustion synthesis as a preparation process to produce fine unagglomered oxides (single or mixed) [1–5] has attracted a good deal of attention. This method exploits an exothermic, redox, rapid and self-sustaining reaction between an oxidant (usually nitrates) and a fuel (urea, glycine, hydrazine and its derivates, etc.). Once initiated, the organic skeleton is destroyed with the evolving of a large amount of gases (mainly H_2O, CO_2, nitrogen oxides).

On the other side, ferroelectromagnetic materials such as bismuth ferrite, ($BiFeO_3$) present a high potential usage in information technology with the emerging of spintronics and sensors [6–8].

In the present paper we report the synthesis of bismuth ferrite by a simple combustion technique, using as starting system $Fe(NO_3)_3 \cdot 9H_2O$–$Bi_5O(OH)_9(NO_3)_4 \cdot 9H_2O$ as oxidizers and glycine or urea as fuels. Because the synthesis of mixed oxide is determined by a combustion reaction, a special attention is paid to the thermal reactivity of the precursor systems. The occurrence of the phase transitions

and evolution of the phase composition with temperature in the obtained oxides, are equally analyzed.

Experimental

The *synthesis* of the BFO precursors was performed using a solid state method. The starting materials of analytical grade $Fe(NO_3)_3 \cdot 9H_2O$ (Merck), $Bi_5O(OH)_9(NO_3)_4 \cdot 9H_2O$ (Merck), glycine (Fluka) and urea (Merck) were used without any further purification. The utilized molar ratios were for $Fe(NO_3)_3 \cdot 9H_2O$–$Bi_5O(OH)_9(NO_3)_4 \cdot 9H_2O$–glycine system 1:5:6, 1:5:8 and 1:5:10, 1:5:12 and, for $Fe(NO_3)_3 \cdot 9H_2O$–$Bi_5O(OH)_9(NO_3)_4 \cdot 9H_2O$–urea system 1:5:12, 1:5:14, 1:5:16, 1:5:18. The compositions were selected in order to obtain fuel lean, stoichiometrically and fuel rich compounds, the stoichiometry being calculated by using the oxidizing valence of metal nitrates and the reducing valence of urea and glycine (fuels). The raw materials mixed ($\sim$30 min) in an agate pestle in order to obtain a homogenous slurry are dried over P_2O_5. Different heating treatments (500, 550, 600 and 650 °C for 3 h) are used in order to obtain the mixed oxides.

The *thermal measurements* were performed on a Q-1500 Paulik-Paulik-Erdey derivatograph, in static air and with sample mass of $\sim$20 mg for precursors and $\sim$50–60 mg for the calcinated oxides. For all measurements the heating rate has been set to 10 K *min^{-1} followed by a cooling performed by switching off the furnace (free cooling). The *X-ray diffraction measurements* were performed at room temperature with a SHIMADZU XRD 6000 diffractometer, using Ni-filtered CuKα radiation ($\lambda = 1.5418$ Å), with a scan step of 0.02° and a counting time of 1 s/step, for 2θ ranged between 20° and 80°. The *FTIR spectra* were obtained by KBr disc technique in the range 400–4000 cm^{-1} using BIO-RAD FTIR 120 infrared spectrophotometer. *TEM investigations* were performed by means of a HRTEM–TECNAI F30 S-Twin ultrahigh resolution electron microscope.

Results and discussion

Characterization of precursors compounds

FT IR investigations of the precursors

The FTIR spectra (Figs. 1a–b, 2a–b) evidenced a coordination of urea and glycine through the oxygen atom. For the urea precursors (Fig. 1a–b) this coordination mode leads to a decrease of the ν_{CO} stretching frequencies in comparison with urea ones (1683 cm^{-1}/$\approx$1634 cm^{-1} for urea/urea precursors) [9, 10]. The corresponding IR spectrum of glycine

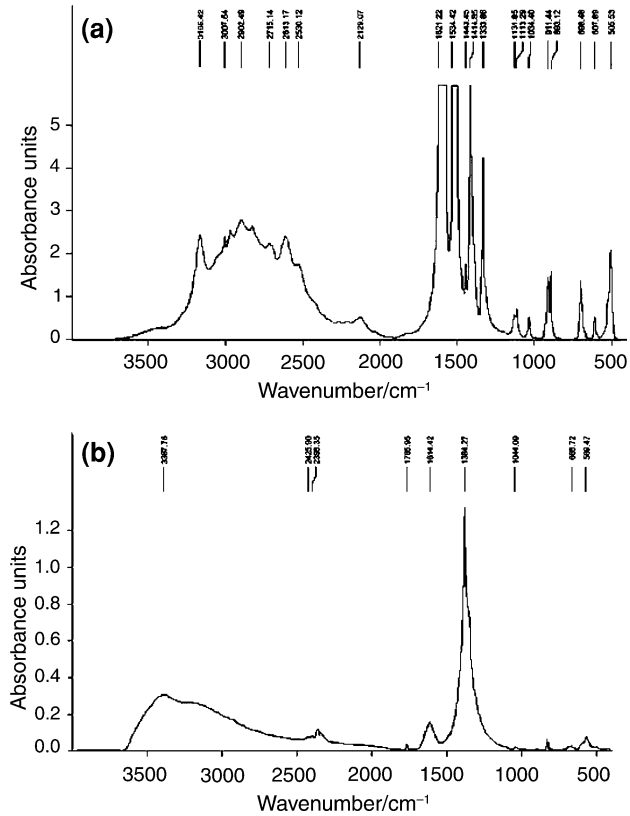

Fig. 1 FTIR spectra of: **a** urea and **b** $Fe(NO_3)_3 \cdot 9H_2O$–$Bi_5O(OH)_9(NO_3)_4 \cdot 5H_2O$–urea (1:5:18) precursor

precursors (Fig. 2a–b) evidences the presence of two bands characteristic for carboxylic group ($\nu_{OCOasym}$ and ν_{OCOsym}). The band characteristic for the $\nu_{OCOasym}$ vibration shifts towards higher frequencies ($\sim$1614 cm^{-1}) and the band assigned to the ν_{OCOsym} vibration towards lower frequencies ($\sim$1360 cm^{-1}). Thus, a value of $\Delta\nu = \nu_{OCOasym} - \nu_{OCOsym} = \sim$253 cm^{-1} suggests a monodentate bonding of this group to the metal ion. Both the precursors systems present bands assigned to uncoordinated NO_3^- identified at $\approx$1384 ($\nu_{asim}(NO_3^-)$ and $\approx$832 cm^{-1}(δNO_3^-) [9]. The last band is completely overlapped in glycine precursors with the one due to ν_{OCOsym} vibration.

Thermal behavior of the precursors systems

The investigated $Fe(NO_3)_3 \cdot 9H_2O$–$Bi_5O(OH)_9(NO_3)_4 \cdot 9H_2O$–glycine/urea precursors undergo in the temperature range 60–350/60–600 °C a stepped decomposition (Figs. 3a–b, 4a–b). Their thermal behavior is fuel nature dependent but practically independent to the fuel content. The presence into the precursor of both reducing (glycine or urea) and oxidizing (NO_3^-) components modifies dramatically their thermal behavior relative to the raw materials (Figs. 5a–b, 6a–b). Several features of their thermal reactivity may be pointed out:

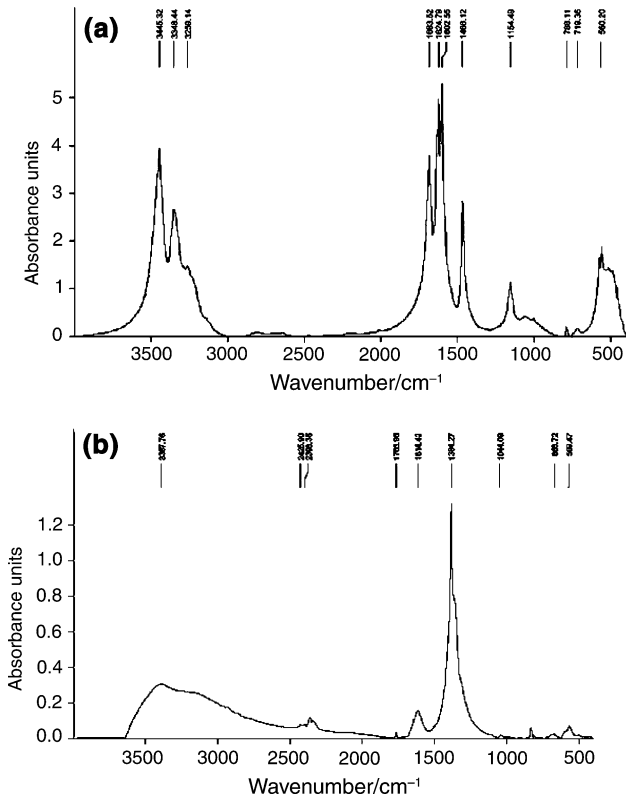

Fig. 2 FTIR spectra of: **a** glycine and **b** $Fe(NO_3)_3 \cdot 9H_2O$–$Bi_5O(OH)_9(NO_3)_4 \cdot 5H_2O$–glycine (1:5:8) precursor

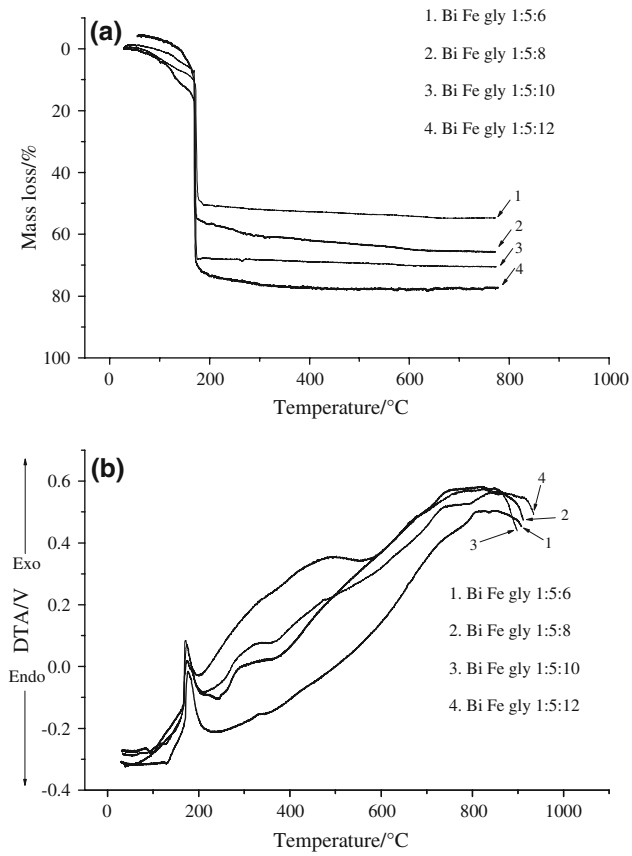

Fig. 3 TG (**a**) DTA (**b**) curves of the $Fe(NO_3)_3 \cdot 9H_2O$–$Bi_5O(OH)_9(NO_3)_4 \cdot 9H_2O$–glycine precursors

A. $Fe(NO_3)_3 \cdot 9H_2O$–$Bi_5O(OH)_9(NO_3)_4 \cdot 9H_2O$–glycine system:

1. The thermal decompositions are described by the existence of three main degradation stages. The first one, ($\sim$60 to $\sim$160 °C, $T_{max\ DTA}$ $\sim$100 °C) characterized by a mass loss of 7–15% and an endothermic effect represents the water evolving. The second decomposition stage is a fast and intensive exothermic process ($\sim$160 to $\sim$185 °C, $T_{max\ DTA}$ $\sim$175 °C, mass loss of 44–65%), and may be attributed to the simultaneous evolving of NO_3^- and glycine. Simultaneously, glycine is oxidized by nitrate anions [11]. The third decomposition stage ($\sim$185 to $\sim$350 °C), accompanied by a medium exothermic effect ($T_{max\ DTA}$ $\sim$300 °C) and a mass loss of $\sim$2–9%, represents the burn up of the remainder carbonaceous residue;
2. The precursors are less stable ($\sim$60 °C) than the free glycine (229 °C), fact which indicates the occurrence of some self-propagating reactions since the start of the decomposition process [12];
3. The small endothermic effects identified at 745 and 818 °C are assigned to Bi_2O_3 $\alpha \rightarrow \delta$ transition and its melting. Such a behavior denotes that not all bismuth is included into mixed oxides. In $Bi_5O(OH)_9(NO_3)_4 \cdot 9H_2O$ raw material, the same transformations are detected at 735.5 °C and 829 °C.

B. $Fe(NO_3)_3 \cdot 9H_2O$–$Bi_5O(OH)_9(NO_3)_4 \cdot 9H_2O$–urea system:

1. Four main decomposition stages of the precursors are identified. The first one, ($\sim$60 to $\sim$145 °C, mass loss 5–8%) associated with two endothermic effects ($T_{max\ DTA}$ $\sim$90 and 140 °C) is attributed to the evolving of water, and urea melting. The second ($\sim$160 to $\sim$200 °C), the third ($\sim$200 to $\sim$320 °C) and the fourth ($\sim$320 to $\sim$600 °C) decomposition stages, characterized by exothermic effects ($T_{max\ DTA}$ $\sim$180, 280 and 460 °C) are assigned to a simultaneously release of urea and decomposition of nitrate ions;
2. The precursors are less stable ($\sim$100 °C) than the free urea (155 °C). On the other hand, the final decomposition temperatures are not drastic decreased in comparison with the raw materials ones;
3. The absence of phase transformations typical for the thermal behavior of Bi_2O_3, proves that unlike

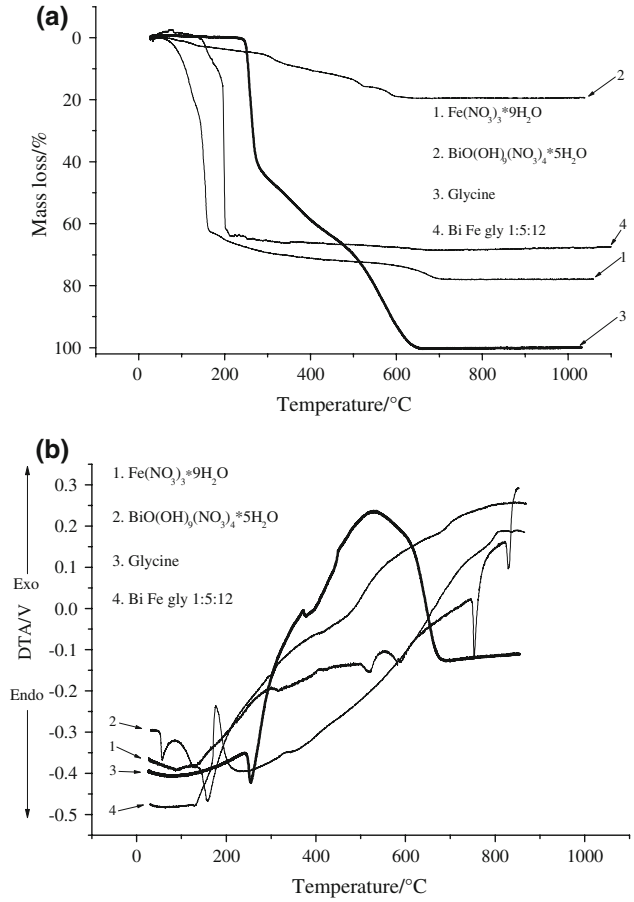

Fig. 4 TG (**a**) and DTA (**b**) curves of the $Fe(NO_3)_3 \cdot 9H_2O$, $Bi_5O(OH)_9(NO_3)_4 \cdot 9H_2O$, glycine and Bi:Fe:glycine = 1:5:12 precursor

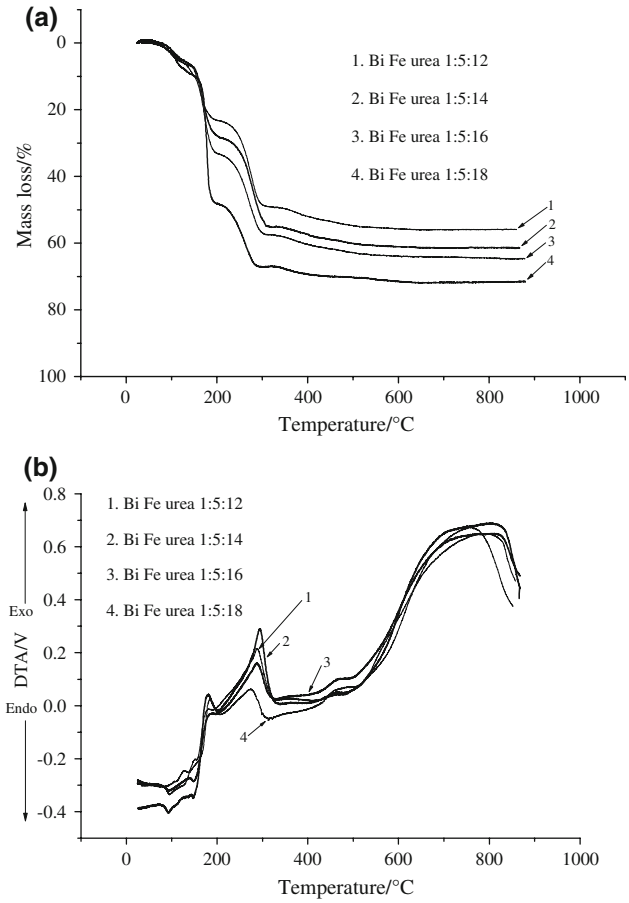

Fig. 5 TG (**a**) and DTA (**b**) curves of the $Fe(NO_3)_3 \cdot 9H_2O$–$Bi_5O(OH)_9(NO_3)_4 \cdot 9H_2O$–urea precursors

glycine system, all bismuth is included into mixed oxides at the end of the thermal decomposition;

4. Small endothermic transitions assigned to the Curie point [13] are detected at ~838 °C for all the investigated systems.

Mixed oxide characterization

Thermal behaviour of the resulted mixed oxides

The thermal analysis experiments performed on oxides samples from ambient temperature to 1050 °C reveal for all oxides a similar behavior (Fig. 7). The first heating ramp depicts the presence of two endothermic effects: the first close to 840 °C corresponding to the ferroelectric Curie temperature (T_C = 830–850 °C) [13] and a second one close to 980 °C corresponding to the melting of oxides. The mentioned endothermic effects are not anymore identified during the second heating cycle due to destruction of $BiFeO_3$ phase by the incongruent melting [14, 15]. The melting points values of the oxides derived from glycine precursors are slightly higher (~10 °C) in comparison with urea derived ones. This trend could be related to the differences in morphology induced by fuels. Also, the oxides generated from urea precursors present higher T_C values, phenomena which could be a consequence of an increasing crystalline order, affirmation in concordance with the X-ray diffraction obtained results.

Successive annealing treatments on the obtained oxides samples may improve crystalline order. We attempted to investigate this hypothesis with a second series of thermal analysis experiments of three successive heating cycles: till above T_C but below the incongruent melting point followed by free cooling. A typical shape of the obtained curves is presented in Fig. 8a–b. A good agreement among the values of the Curie temperature of the first cycle is obtained, taking into account the error of 1 K for temperature measurements with our mentioned thermal analysis equipment. The differences between the Curie temperature values obtained during the heating and respectively cooling procedures, originate from the different heating and cooling rates. On the other hand, for all the investigated samples, the Curie temperature decreases with the number of

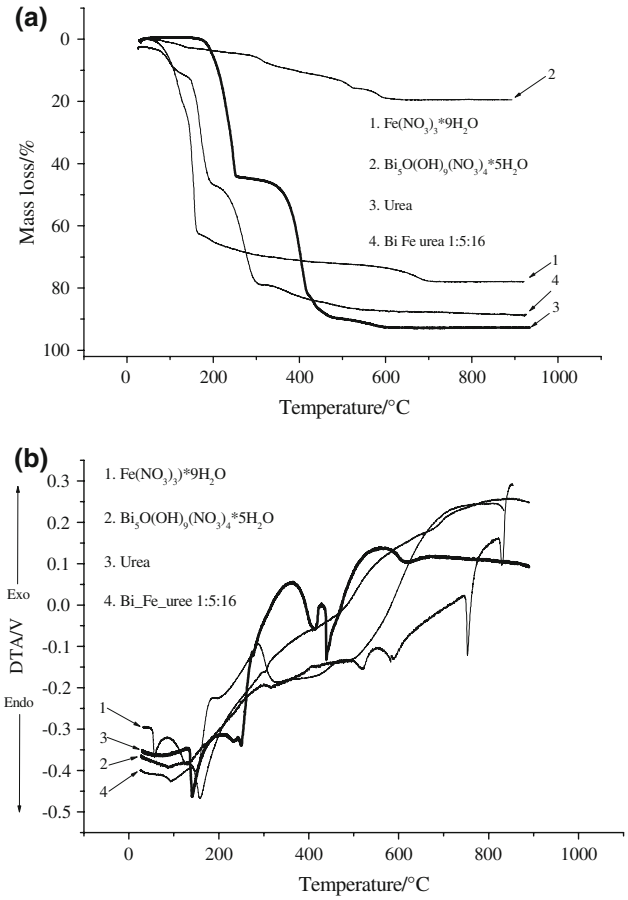

Fig. 6 TG (**a**) and DTA (**b**) curves of the $Fe(NO_3)_3 \cdot 9H_2O$, $Bi_5O(OH)_9(NO_3)_4 \cdot 9H_2O$, urea and Bi:Fe:urea = 1:5:16 precursor

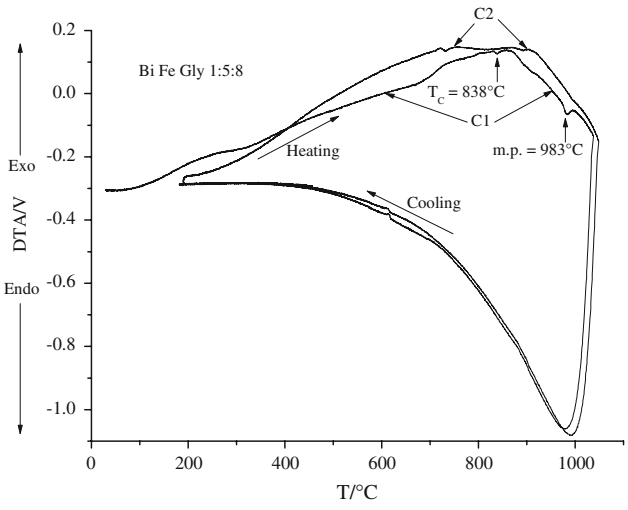

Fig. 7 DTA curves for $BiFeO_3$ obtained from $Bi_5O(OH)_9(NO_3)_4 \cdot 5H_2O$:$Fe(NO_3)_3 \cdot 9H_2O$:glycine = 1:5:8. C1, C2: first/second heating/cooling cycle

annealing treatments. Such an effect could be related to the deterioration of $BiFeO_3$ crystalline order, deterioration induced either by bismuth vaporization [16, 17] or by

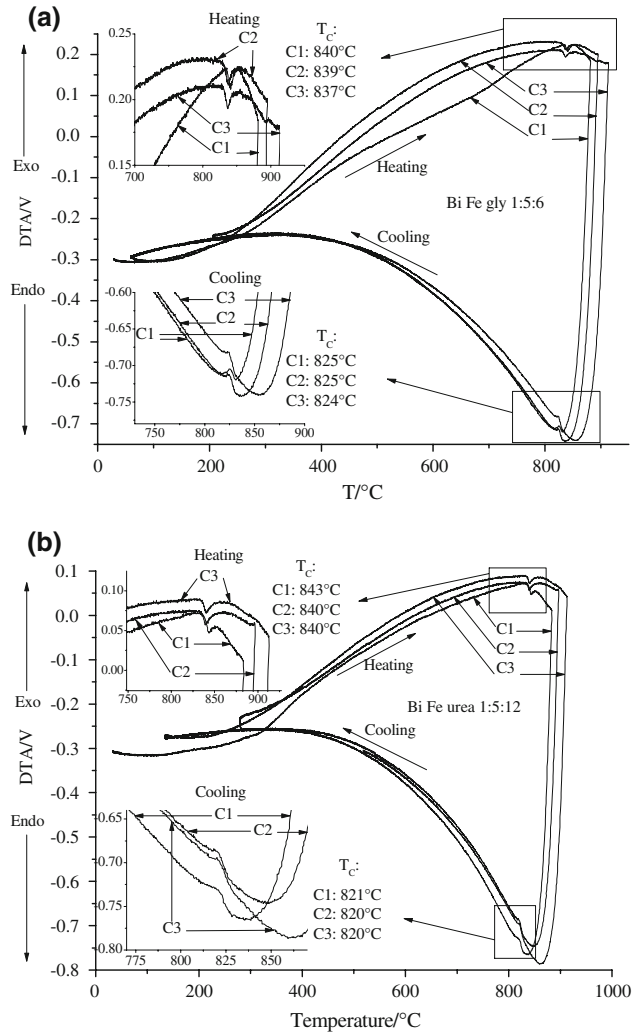

Fig. 8 **a**, **b** Influence of successive annealing treatments on Curie temperatures of $BiFeO_3$ obtained using: **a** $Bi_5O(OH)_9(NO_3)_4 \cdot 5H_2O$:$Fe(NO_3)_3 \cdot 9H_2O$:glycine = 1:5:6 and **b** $Bi_5O(OH)_9(NO_3)_4 \cdot 5H_2O$:$Fe(NO_3)_3 \cdot 9H_2O$:urea = 1:5:12. C1–C3: first to third heating/cooling cycle

oxygen vacancies generation [15–18]. The last factor is highly probable, since the oxygen vacancies in $BiFeO_3$ may be compensated by Fe^{III}/Fe^{II} valence fluctuation [17–20]. Indeed, this hypothesis appears to be sustained by a slight mass loss observed for each sample from TG curves during every heating/cooling cycle. The complexity of this problem requires a dedicated study which is in progress and will be reported further.

Phase composition and morphology of the mixed oxide powders

Although the evolution of both the interaction processes and the phase composition has several peculiarities function of the metallic cations/fuels ratio variation, several general conclusions may be pointed out for each investigated system.

For the powders prepared by using glycine as fuel and annealed at different temperatures show the evolution of both the interaction processes and the phase composition. At 500 °C, beside the major perovskite $BiFeO_3$ phase, some non-equilibrium compounds such as $Bi_2Fe_4O_9$ and $Bi_{36}Fe_2O_{57}$ were also detected as secondary phases at the detection limit (Fig. 9). This result is quite different in comparison with the phase composition of the oxide powder prepared in the same annealing conditions from $Bi(NO_3)_3 \cdot 9H_2O$ and $Fe(NO_3)_3 \cdot 9H_2O$ using also glycine as fuel. In the last one $BiFeO_3$ was only a minor phase, as we reported elsewhere [21]. The rise of the annealing temperature in the temperature range of 500–650 °C determines the gradual consumption of the secondary $Bi_{36}Fe_2O_{57}$ phase. Simultaneously with this process, in the mentioned temperature range, an increase of the amounts of both $BiFeO_3$ perovskite and $Bi_2Fe_4O_9$ compound was also pointed out by the enhancement of the characteristic diffraction peaks. Thus, after a thermal treatment of 3 h at 650 °C a double-phase powder consisting of well-crystallized $BiFeO_3$ perovskite with a rhombohedral $R\bar{3}m$ symmetry and $Bi_2Fe_4O_9$ was obtained (Fig. 9). The secondary $Bi_2Fe_4O_9$ phase, detrimental to the electrical behavior of the $BiFeO_3$ ceramics, increase with the increase of fuel amount, a smaller amount of the phase being detected for $Bi_5O(OH)_9(NO_3)_4 \cdot 5H_2O$–$Fe(NO_3)_3 \cdot 9H_2O$–glycine = 1:5:6 system.

Unlike the powders prepared with glycine, in the case of the powders synthesized using urea as fuel, a faster evolution toward a single phase composition with the temperature rise was pointed out by the X-ray diffraction patterns (Fig. 10). It is worthy to mention that, for these oxide powders, the formation of the perovskite $BiFeO_3$ phase is almost completed at 500 °C. Only some traces of $Bi_{36}Fe_2O_{57}$ were identified at the detection limit. The further increase of the annealing temperature does not influence significantly the phase composition, so that the powders thermally treated at temperatures ranged between 600 and 650 °C were almost single phase, irrespective of the amount of the fuel.

The influence of the metallic cations/fuels ratio on the phase composition, particle sizes, morphology and surface area will be presented in a further paper.

TEM analysis performed on the $BiFeO_3$ nanopowder synthesized by using glycine as fuel and thermally treated at 500 °C for 3 h revealed the presence of small particles with an average size of ~33 nm and with a high tendency to form strongly 3D-interconnected aggregates (Fig. 11a). For the $BiFeO_3$ powder resulted by using urea as fuel and thermally treated in the same conditions, the TEM image (Fig. 11b) indicates the presence of rather isolated polycrystalline agglomerates with an average size of ~100 nm. Since it was very hard to disperse this powder and because of the strongly bonded agglomerates, it was difficult to estimate an average particle size even by TEM investigations. However, these agglomerates seem to consist of small particles of various sizes, the smallest noticed here having around ~14 nm as indicated by the arrow in the TEM image (Fig. 11b). These observations are in good agreement with the SEM results obtained for the $BiFeO_3$ powders prepared by using the same fuels, but different Bi precursor and different precursors ratio [21].

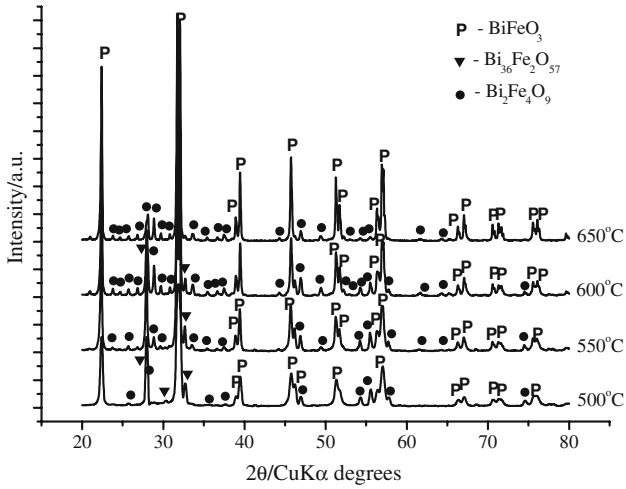

Fig. 9 Room temperature X-ray diffraction patterns of the $BiFeO_3$ powders prepared from $Bi_5O(OH)_9(NO_3)_4 \cdot 5H_2O$ and $Fe(NO_3)_3 \cdot 9H_2O$ using glycine as fuel (1:5:8) and annealed for 3 h at various temperatures ($BiFeO_3$—JCPDS no. 73-0548; $Bi_2Fe_4O_9$—JCPDS no. 25-0090; $Bi_{36}Fe_2O_{57}$—JCPDS no. 42-0181)

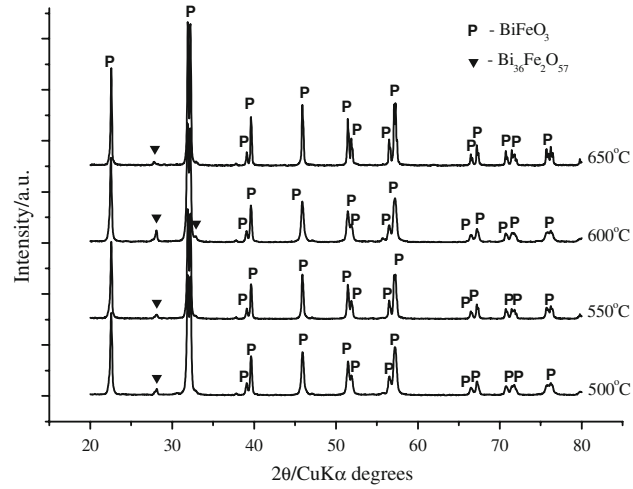

Fig. 10 Room temperature X-ray diffraction patterns of the $BiFeO_3$ powders prepared from $Bi_5O(OH)_9(NO_3)_4 \cdot 5H_2O$ and $Fe(NO_3)_3 \cdot 9H_2O$ using urea as fuel (1:5:18) and annealed for 3 h at various temperatures ($BiFeO_3$—JCPDS no. 73-0548; $Bi_{36}Fe_2O_{57}$—JCPDS no. 42-0181)

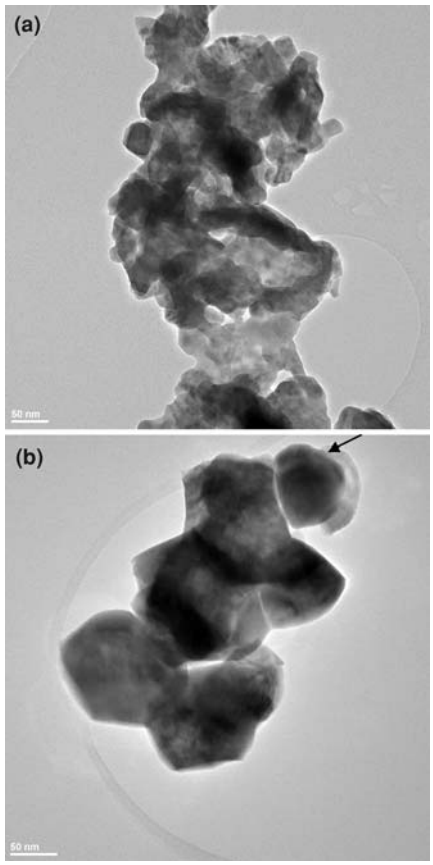

Fig. 11 TEM images of the $BiFeO_3$ powders thermally treated at 500 °C for 3 h and synthesized by using as fuel: **a** glycine and **b** urea

Conclusions

Combustion method represents a suitable route in the synthesis of nanosized $BiFeO_3$ at temperatures lower than 650 °C. The fuel nature, glycine or urea strongly influences the thermal behavior of the precursors, solid state mechanism and some characteristics of the resulted oxides (phase composition, thermal stability). The formation of the major perovskite phase is more rapid into the oxides derived from urea precursors in comparison with glycine ones, so that, even at lower temperatures ($\sim$500 °C), an obvious trend to a single phase composition was noticed. In the case of the oxides derived from glycine precursors, some decomposition processes with formation of $Bi_2Fe_4O_9$ take place, so that the evolution toward a single phase composition is slowed down.

The values of the Curie temperature identified by DTA curves decrease with the number of annealing treatments, effect that may be related to the deterioration of crystalline order of $BiFeO_3$ induced either by bismuth vaporization or oxygen vacancies generation. All the $BiFeO_3$ samples, present an incongruent melting, the oxides derived from glycine precursors exhibiting a slightly higher ($\sim$10 °C) melting point in comparison with urea derived ones.

TEM analysis reveals a high tendency to form strongly 3D-interconnected aggregates. Particles with an average size of $\sim$33 nm were identified in the case of glycine derived oxides, while in urea one polycrystalline agglomerates with an average size of $\sim$100 nm.

References

1. Fu YP, Lin CH, Hsu CS. Preparation of ultrafine CeO_2 powders by microwave-induced combustion and precipitation. J Alloy Compd. 2005;391:110–4.
2. Kalai Selvan R, Augustin CO, Berchmans LJ, Saraswaithi R. Combustion synthesis of $CuFe_2O_4$. Mater Res Bull. 2003;38: 41–54.
3. Wang SF, Gu F, Lü MK, Cheng XF, Zou WG, Zhou GJ, et al. Synthesis and photoluminescence characteristics of Dy^{3+} doped ZnA_2O_4 nanocrystals via combustion process. J Alloy Compd. 2005;394:255–8.
4. Sekal MMA, Patil KC. Combustion synthesis and fine particle dielectric oxide materials. J Mater Chem. 1992;2;739–44.
5. Minami T, Patil KC. Solution combustion synthesis of nanoscale oxides and their composites. Mater Phys Mech. 2001;4: 134–47.
6. Wang J, Neaton JB, Zheng H, Nagarajan V, Ogale SB, Liu B, et al. Epitaxial $BiFeO_3$ multiferroic thin film heterostructures. Science. 2003;299:1719–22.
7. Fiebig M, Lottermoser T, Frohlich D, Goltsev AV, Pisarev RV. Observation of coupled magnetic domains. Nature. 2002;419: 818–20.
8. Kumar MM, Palkar VR, Srinivas K, Suryanarayana SV. Ferroelectricity in a pure $BiFeO_3$ ceramics. Appl Phys Lett. 2000;76: 2764–6.
9. Nakamoto K. Infrared spectra of inorganic compounds. New York: Wiley; 1978.
10. Penland RB, Mizushima S, Curran C, Qugliana JV. Infrared absorption spectra of some inorganic coordination complexes: X. Studies of some metal-urea complexes. J Am Chem Soc. 1957;79:1575–8.
11. Yan CH, Xu ZG, Xheng FX, Wang ZM, Sun LD, Liao CS, et al. Nanophase $CoFe_2O_4$ prepared by a combustion method. Solid State Commun. 1999;111:287–91.
12. Carp O, Patron L, Diamandescu L, Reller A. Thermal decomposition study of the coordination compound $[Fe(urea)_6](NO_3)_3$. Thermochim Acta. 2002;390:169–77.
13. Iakovlev S, Solterbeck CH, Kuhnke M, Es-Souni M. Multiferroic $BiFeO_3$ thin films processed via chemical solution deposition. Structural and electrical characterization. J Appl Phys. 2005;97: 094901-06.
14. Koizumi H, Niizeki N, Ikeda T. An X-ray study on Bi_2O_3–Fe_2O_3 system. J Appl Phys. 1964;3:495–6.
15. Speranskaya EI, Skorikov VM, Rode EY, Serekhova VA. The phase diagram of the system bismuth oxide-ferric oxide. Izv Akad Nauk SSSR, Ser Khim. 1965;5:905–6.
16. Lebeugle D, Colson D, Forget A, Viret M, Bonville P, Marucco JF, et al. Room-temperature coexistence of large electric polari-

zation and magnetic order in $BiFeO_3$ single crystals. Phys Rev B. 2007;6:24116-8.
17. Habouti S, Solterbeck CH, Es-Souni M. UV assisted pyrolysis of solution deposited $BiFeO_3$ multiferroic thin films. Effects on microstructure and functional properties. J Sol-Gel Sci Technol. 2007;242:257–63.
18. Singh VR, Dixit A, Garg A, Agrawal DC. Effect of heat treatment on the structure and properties of chemical solution processed multiferroic $BiFeO_3$ thin films. Appl Phys A. 2008;90: 197–202.
19. Palkar VR, John J, Pinto R. Observation of saturated polarization and dielectric anomaly in magnetoelectric $BiFeO_3$ thin films. Appl Phys Lett. 2002;80:1628–30.
20. Wang YP, Zhou L, Zhang MF, Chen XY, Liu JM, Liu ZG. Room-temperature saturated ferroelectric polarization in $BiFeO_3$ ceramics synthetized by a rapid liquid phase. Appl Phys Lett. 2004;84:1731–3.
21. Paraschiv C, Jurcă B, Ianculescu A, Carp O. Synthesis of nanosized bismuth ferrite ($BiFeO_3$) by a combustion method starting from $Fe(NO_3)_3{\cdot}9H_2O$–$Bi(NO_3)_3{\cdot}9H_2O$–glycine or urea systems. J Therm Anal Calorim. 2008;94:411–6.